Research Square

Preprints are preliminary reports that have not undergone peer review.
They should not be considered conclusive, used to inform clinical practice,
or referenced by the media as validated information.

A Cost–Benefit–Reliability (CBR) Framework for Additive and Hybrid Manufacturing of Electronic Assemblies

Martin P Goetz

martin.goetz@ngc.com

Northrop Grumman Mission Systems Baltimore: Northrop Grumman Mission Systems
https://orcid.org/0009-0000-8426-3411

Philip Lovell

Northrop Grumman Mission Systems Baltimore: Northrop Grumman Mission Systems

Research Article

Keywords: Additive manufacturing, hybrid manufacturing, defense electronics, reliability engineering, cost modeling, conformal antennas, DFAM

Posted Date: October 29th, 2026

DOI: https://doi.org/10.21203/rs.3.rs-11353326/v1

License: This work is licensed under a Creative Commons Attribution 4.0 International License.
Read Full License

Additional Declarations:

Declaration of interests

The authors declare that they have no known competing financial interests or personal relationships that could have appeared to influence the work reported in this paper.

The authors declare the following financial interests/personal relationships which may be considered as potential competing interests:

A Cost–Benefit–Reliability (CBR) Framework for Additive and Hybrid Manufacturing of Electronic Assemblies

Martin P. Goetz and Philip A. Lovell
Northrop Grumman Mission Systems, Linthicum, MD 21090
martin.goetz@ngc.com ORCID: 0009-0000-8426-3411

Abstract

Additive manufacturing (AM) processes for metals, polymers, and ceramics are increasingly applied to high-reliability electronic assemblies. These applications require manufacturing routes that meet aggressive size, weight, and power (SWaP) targets while satisfying environmental standards like MIL-STD-810H and MIL-STD-883. This paper proposes a reliability-aware Cost–Benefit–Reliability (CBR) framework to evaluate when additive and hybrid manufacturing provide measurable advantages over conventional methods. A taxonomy of relevant AM technologies is mapped to specific electronic functions and material properties. Decision criteria—including geometric complexity, production volume, lead time, and failure-mode mitigation—are quantified using the CBR model. Four defense-electronics case studies demonstrate quantitative trade-offs in SWaP, cost, and reliability across metal and hybrid workflows. AM-specific failure mechanisms are addressed through design-for-additive-manufacturing (DfAM) guidelines and qualification pathways. A correlation-aware Monte Carlo formulation and global sensitivity analysis show that AM failure rate and nonrecurring engineering (NRE) cost are the dominant drivers of CBR decision uncertainty. The results indicate that additive and hybrid manufacturing are most advantageous for low-volume, high-complexity assemblies, and that process qualification is essential for successful adoption.

Keywords: Additive manufacturing, hybrid manufacturing, defense electronics, reliability engineering, cost modeling, conformal antennas, DFAM.

1.0 INTRODUCTION

High-reliability electronic assemblies for aerospace and defense applications—such as avionics, radar front ends, and unmanned-air-vehicle (UAV) mission electronics—must simultaneously achieve aggressive SWaP targets, electromagnetic performance, and long lifetime under harsh environmental loads. Conventional manufacturing routes based on planar printed-circuit boards (PCBs), machined housings, and assembled interconnects are often constrained by tooling, geometric limitations, and multi-piece assembly complexity. As platform requirements tighten and production volumes remain relatively low, these conventional routes can become uneconomical or may fail to exploit available geometric freedom for performance improvements.

Additive manufacturing (AM) and hybrid manufacturing (AM combined with subtractive or joining processes) offer new pathways for fabricating such assemblies. Metal AM processes, including laser-based powder-bed fusion (LPBF) and hybrid additive–subtractive techniques, have been used to produce conformal RF apertures, integrated heat sinks, and lightweight structures [1], [3], [4], [9], [12], while ink-jet and aerosol-jet printing enable fine-feature conductors and dielectrics for RF and sensing functions [1], [2]. Ceramic AM, including stereolithography, provides high-dielectric-constant substrates and packages for high-frequency applications [17]. Demonstrations of additively manufactured conformal antennas, cavity-backed arrays, and RF subsystems indicate that AM can achieve performance comparable to or better than conventional counterparts [1], [4]–[6], [9].

Despite this progress, the adoption of AM and hybrid routes in production high-reliability electronics remains limited. For many programs, the central question is not whether a specific component can be printed, but whether an AM or hybrid route provides sufficient benefit—geometric, performance, or logistical—to justify changes in cost

structure, qualification effort, and reliability risk. There is currently no widely used quantitative framework to answer this question at the assembly level, accounting simultaneously for SWaP, cost, reliability, and environmental qualification.

This paper addresses that gap by proposing a reliability-aware Cost–Benefit–Reliability (CBR) framework for comparing AM / hybrid and conventional manufacturing routes for high-reliability electronic assemblies. The framework combines:

- An AM process and material taxonomy tailored to electronic functions.
- A multi-criteria benefit metric aggregating SWaP reduction, functional integration, and performance improvements.
- A total cost of ownership (TCO) model incorporating unit, non-recurring engineering (NRE), logistics, and reliability-related costs.
- A reliability factor based on effective mission-time failure rates, derived from accelerated testing and literature data [3], [10], [11].
- A correlation-aware uncertainty and sensitivity analysis using Gaussian copulas and variance-based global sensitivity indices [10], [14].

The contributions of this work are:

- A **CBR framework** that couples SWaP, functional integration, cost, and reliability outcomes for additive, hybrid, and conventional manufacturing routes in high-reliability electronics.
- A **process–material capability map** and representative property data for AM processes used in electronic assemblies, grounded in literature and internal trials [1]–[3], [9], [11], [17].
- A **correlation-aware uncertainty and sensitivity analysis** that identifies AM failure rate and NRE cost as dominant drivers of decision uncertainty in low-volume defense-electronics scenarios [10], [14].
- Four manufacturing **case studies**—conformal antenna housing, integrated power-distribution module, ruggedized microwave package, and embedded health-monitoring sensor—that demonstrate the application of the framework and highlight specific AM and hybrid process levers [5], [6], [10], [12].

The remainder of this paper is organized as follows. Section 2 summarizes the requirements and constraints for high-reliability electronic assemblies and motivates the use of AM and hybrid routes. Section 3 reviews AM technologies and material properties relevant to electronics. Section 4 presents the CBR decision framework. Section 5 presents four case studies, introduces the cost–benefit analysis and uncertainty/sensitivity study, and summarizes DfAM guidelines. Section 6 discusses AM-specific reliability mechanisms and qualification pathways. Section 7 outlines future research directions, and Section 8 concludes.

2.0 DEFENSE-ELECTRONICS REQUIREMENTS

High-reliability electronic assemblies in defense and aerospace systems are constrained by mission, platform, and environmental requirements. Representative requirements include limits on mass per bay, envelope volume, board thickness, and power dissipation, as well as constraints on radar cross-section (RCS), thermal gradients, mechanical shock and vibration, radiation tolerance, and lifecycle reliability [7], [8], [10]. Table 1 summarizes typical requirements and identifies conventional-manufacturing limitations and potential AM advantages for each.

Table 1. Defense-electronics requirements and corresponding additive-manufacturing opportunities.

Requirement	Typical Specification	CM Limitation	Potential AM Advantage
SWaP	< 20 kg per avionics bay; board thickness ≤ 0.4 mm	Planar PCBs cannot achieve conformal volume reduction	Conformal 3D interconnects, integrated housings
EMC / Low-Observable (LO)	RCS (Radar Cross-Section) reduction > 30 dB	Discrete metallic components increase scattering	Graded-dielectric composites, embedded antennas
Thermal Management	$\Delta T \leq 30$ °C under 50 W dissipation	Heat sinks limited to standard shapes	Lattice infill, embedded micro-channels
Mechanical Shock/Vibration	20 g, 2000 Hz (MIL-STD-810H)	Fragile solder joints, board flexure	Monolithic structures, tailored anisotropy
Radiation Hardness	Total ionizing dose (TID) ≥ 100 krad (Si)	Standard polymers degrade	Ceramics, metal-matrix composites
Lifecycle Reliability	$> 10^6$ h MTBF	Process-induced variability in copper plating	Process control, in-situ monitoring
Lead-Time / Low-Volume	100–500 units per year	Tooling costs dominate	No-tool AM enables rapid, on-demand production
Logistics / Supply Chain	Global theater deployment; limited spares	Long lead times, single-source constraints	Distributed manufacturing, digital twins

The limits in Table 1 are consistent with typical MIL-STD-810H environmental profiles and MIL-STD-883 microcircuit requirements [7], [8]. They illustrate why high-reliability electronics are a demanding application domain for advanced manufacturing. Geometric complexity and conformal surfaces are often required to achieve SWaP and low-observable performance, while low-volume, high-mix production and global logistics constraints make conventional tooling and supply chains comparatively inflexible. Heat dissipation and mechanical robustness constraints drive complex heat-sink designs and monolithic or quasi-monolithic packaging.

These characteristics motivate a manufacturing approach in which AM and hybrid routes are considered alongside conventional machining and PCB-based routes. AM can realize conformal housings, internal cooling channels, and integrated interconnects, and can reduce NRE and lead time for low-volume, high-complexity assemblies. However, these benefits must be weighed against process-specific reliability risks, qualification effort, and cost structures.

3.0 ADDITIVE MANUFACTURING TECHNOLOGIES FOR ELECTRONICS

3.1 Process Taxonomy and Functional Capabilities

AM processes relevant to electronic assemblies can be grouped into several families, each with distinct trade-offs in resolution, build rate, material palette, and achievable features [1]–[3], [9]:

- **Material extrusion (FDM/FFF)**, including conductive polymer composites (e.g., Cu-filled thermoplastics, CNT-reinforced PEEK), offers moderate resolution and moderate electrical conductivity, with good mechanical robustness. These processes are suited to structural housings, low-current interconnects, and structural electronics [1], [3].
- **Ink-jet and aerosol-jet (AJ) printing** deposit conductive inks (e.g., Ag or Cu nanoparticles) and dielectric inks with fine lateral resolution, supporting RF transmission lines, conformal antenna patterns, fine-pitch interconnects, and sensors on complex surfaces [1], [2].
- **Laser-based powder-bed fusion (LPBF)** of metals such as Cu, Al, and Ti produces high-conductivity carriers and structural components, including waveguides, heat sinks, and RF housings [3], [4].
- **Ceramic stereolithography (SLA)** enables high-dielectric-constant substrates and packages (e.g., Al_2O_3), which are useful for filters, resonators, and radome-like structures [17].
- **Direct laser writing / two-photon polymerization (DLW/TPP)** achieves sub-10-μm features for micro-scale antenna elements, vias, and sensing channels, albeit at low build rates [1], [9].

Table 2. AM process taxonomy for defense electronics applications.* Pure Cu LPBF requires optimized laser sources (e.g., green lasers) and controlled atmospheres to achieve these properties.

AM Process	Typical Materials	Resolution	Build Rate	Key Electronic Features
Material Extrusion (FDM/FFF)	Conductive polymer composites (Cu-PEI), thermoplastics, high-temperature ULTEM®	100–300 μm (layer)	5–30 mm^3/s	Simple conductors, structural housings, monolithic multi-layer low-dielectric planar radiator circuit boards, AM SMP RF connectors
Ink-Jet / Aerosol-Jet (AJ)	Silver nanoparticle inks, CNT inks, dielectric inks	10–50 μm (droplet)	0.5–2 mm^3/s	Fine traces, fine-pitch interconnects, RF antenna patterns
Laser-Based Powder-Bed Fusion (LPBF)*	Cu, Al, Ti alloys; ceramics (Al_2O_3, SiC)	20–50 μm	5–15 mm^3/s	High-conductivity metal carriers, RF waveguides
Direct Laser Writing (DLW) / Two-Photon Polymerization (TPP)	Photopolymers with metal precursors, ceramic slurries	≤ 5 μm	< 1 mm^3/s	Micro-antenna elements, high-aspect-ratio vias
Binder Jetting + Sintering	Cu, Ni, Fe powders; ceramic green bodies	30–100 μm	10–30 mm^3/s	Bulk metal parts, integrated heat sinks
Hybrid AM/Subtractive (e.g., CNC-Milling after LPBF)	Metals, composites	≤ 10 μm (post-finish)	—	Precise RF cavities, conformal waveguides

Table 2 summarizes these processes, their typical materials, resolution ranges, and key electronic features. A process–material capability matrix (Figure 1) positions the AM process families along axes of geometric resolution

and primary electronic function (structural/thermal vs RF/interconnect/sensing), highlighting regions where hybrid AM workflows are especially promising—for example, LPBF copper housings with inkjet-printed feed networks and dielectric layers [1], [4]–[6], [9].

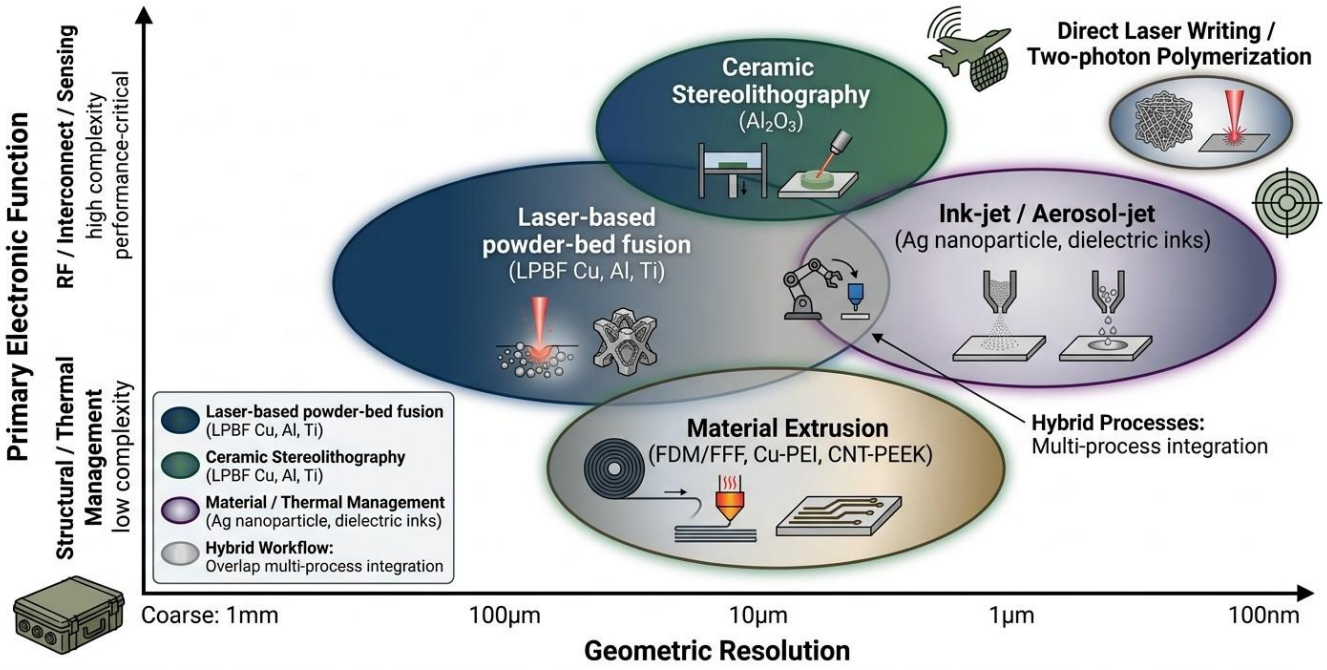


Fig. 1. Process–material capability matrix for additive manufacturing routes used in electronic assemblies, highlighting regions of overlap between conductive and dielectric AM processes.

3.2 Material–Process–Property Relationships

The effectiveness of AM routes in electronic assemblies depends on electrical conductivity, dielectric and thermal properties, and mechanical integrity. Table 3 summarizes representative material properties for selected AM materials drawn from [1]–[3], [9], [11], [17], and internal trials: Cu-filled polymers, Ag nanoparticle inks, LPBF copper, ceramic SLA (Al_2O_3), Ti-6Al-4V, and CNT-reinforced thermoplastics.

Table 3. Representative material properties for additive-manufactured electronics.

Material	Process	σ (S/m)	ε_r (25 °C)	k (W/m·K)	Typical Yield Strength (MPa)
Cu-PEI composite (30 wt % Cu)	FDM	4.8×10^4	3.2	0.75	45
Ag nanoparticle ink (post-cure)	AJ	5.5×10^6	3.6	0.45	—
Pure Cu (LPBF, HIP)	LPBF	5.8×10^7	1.0	386	250
Al_2O_3 (ceramic stereolithography)	SLA	—	9.5	30	350
Ti-6Al-4V (LPBF + stress-relief)	LPBF	—	9.0	6.7	880
CNT-PEEK composite	FDM	2.3×10^5	2.8	0.9	95

Several trends in Table 3 are critical for manufacturing decisions:

- Printed metal traces (e.g., Ag nanoparticle inks) typically exhibit conductivities below bulk metals; process and post-processing conditions (sintering temperature/time, photonic sintering) strongly affect reliability under thermal cycling and mechanical stress [2], [11].
- The dielectric constant of polymer and ceramic formulations can be tuned via filler loading to support graded-index substrates and low-observable radomes [1], [9], [17].
- Metal-filled polymers can provide moderate thermal conductivity suited for low to medium power densities, but high-heat-flux components generally require LPBF metals or hybrid metal inserts to achieve acceptable temperature gradients [3], [10].
- LPBF metals and ceramic SLA parts provide mechanical strength suitable for rugged housings and structural components, but are susceptible to porosity, anisotropic residual stresses, and surface-roughness-induced losses if not properly controlled [3], [14].

In the case studies of Section 5, AM routes are selected directly from this taxonomy: LPBF copper with printed feed networks for conformal antenna housings, hybrid LPBF-plus-printed-interconnect workflows for power-distribution modules, ceramic stereolithography with metallization for microwave packages, and DLW-based channels for embedded sensing. The property ranges in Table 3 are used to parameterize the benefit and reliability terms in the CBR model.

4.0 DECISION FRAMEWORK – WHEN AM IS BENEFICIAL

4.1 Cost–Benefit–Reliability (CBR) Index

To compare AM/hybrid and conventional manufacturing routes, we define a scalar Cost–Benefit–Reliability index Ψ:

$$\Psi = \frac{B \cdot R}{C_{\text{norm}}} \quad (1)$$

where B is a dimensionless benefit score, R is a reliability factor (probability of survival over the required mission time), and $C_{\text{norm}}$is a normalized total cost of ownership (TCO) ratio between AM and conventional routes.

The benefit score B aggregates normalized SWaP improvements, part-count reduction (functional integration), and performance gains:

$$B = \alpha_1 \Delta\text{SWaP} + \alpha_2 \Delta N + \alpha_3 \Delta\eta \quad (2)$$

where ΔSWaP, ΔN, and Δη represent normalized changes in SWaP, part count, and a performance metric (e.g., antenna gain, thermal resistance, insertion loss) relative to the conventional baseline, and $\alpha_1, \alpha_2, \alpha_3$are non-negative weighting coefficients with $\alpha_1 + \alpha_2 + \alpha_3 = 1$.

The normalized cost ratio $C_{\text{norm}}$is defined as:

$$C_{\text{norm}} = \frac{C_{\text{AM}}}{C_{\text{CM}}} = \frac{C_{\text{U,AM}} Q + C_{\text{NRE,AM}} + C_{\text{L,AM}}}{C_{\text{U,CM}} Q + C_{\text{NRE,CM}} + C_{\text{L,CM}}} \quad (3)$$

where C_U is unit manufacturing cost, C_NRE is non-recurring engineering cost, C_L is logistics and sustainment cost, and Q is production quantity. The total cost difference ΔTCO = TCO_CM − TCO_AM complements Ψ by indicating whether AM also offers absolute TCO savings [10].

Values $\Psi > 1$ indicate that AM/hybrid routes provide a net advantage relative to conventional manufacturing, accounting for benefits, reliability, and cost; $\Psi = 1$ denotes a break-even condition, and $\Psi < 1$ favors conventional routes.

4.2 Reliability Factor

For many high-reliability electronics, a constant failure rate is a reasonable approximation over the mission lifetime [10], [11]. In such cases, the reliability factor R is modeled using an exponential:

$$R = \exp\left(-\lambda t_{\text{req}}\right) \quad (4)$$

where λ is an effective mission-time failure rate (λ_AM or λ_CM) and $t_{\text{req}}$is the required operational time. When data suggest non-constant hazard rates (e.g., early-life failures or wear-out), a Weibull model with scale parameter η_W and shape parameter β can be used:

$$R = \exp\left[-\left(\frac{t_{\text{req}}}{\eta_W}\right)^{\beta}\right] \quad (5)$$

In this work, effective λ_AM and λ_CM for the case studies are estimated from a combination of internal accelerated-life test data and published studies on printed conductors and AM metals [3], [10], [11]. Temperature-acceleration factors and environmental stress profiles derived from MIL-STD-810H and MIL-STD-883 are used to relate accelerated test conditions to use conditions [7], [8].

4.3 Weighting Coefficients and Decision Thresholds

The coefficients $\alpha_1, \alpha_2, \alpha_3$reflect platform-specific priorities among SWaP, part-count reduction, and performance metrics. We obtained representative weights for the case studies using the Analytic Hierarchy Process (AHP) pairwise comparisons conducted with cross-functional teams [10]:

- SWaP was typically rated "strongly more important" than performance improvements and "very strongly more important" than part-count reduction.
- The resulting normalized weights were approximately $\alpha_1 \approx 0.55$, $\alpha_2 \approx 0.15$, $\alpha_3 \approx 0.30$, with AHP consistency ratios below 0.1.

Three derived metrics guide interpretation of Ψ:

- **Geometric complexity (GC):** quantified via surface-to-volume ratio and internal channel density; high GC (>~0.03 mm^{-1}) tends to favor AM for conformal and integrated designs.
- **Lead-time sensitivity (LT):** $LT = t_{\text{req}}/t_{\text{tool}}$; values LT < 0.5 indicate that elimination of tooling via AM/hybrid routes can be decisive.
- **Reliability margin (RM):** RM = MTBF_target − MTBF_AM; AM is acceptable when RM ≥ 0 and R_AM over the mission window remains above program thresholds.

These thresholds are evaluated for each case study to assess whether AM/hybrid routes are attractive under program constraints.

5.0 CASE STUDIES AND COST-BENEFIT ANALYSIS

5.1 Quantitative Framework Evaluation Under Uncertainty

To validate the reliability-aware Cost–Benefit–Reliability (CBR) framework and evaluate the scalar index Ψ under realistic operational conditions, a baseline Monte Carlo simulation (n = 10,000 trials) was constructed using a Gaussian copula to model known dependencies [14]. Costs are modeled using asymmetric lognormal or normal distributions to capture real-world engineering risks, while effective mission-time failure rates λ_{AM} and λ_{CM} are parameterized using Weibull-derived effective rates rooted in accelerated lifecycle testing and environmental stress profiles [10], [11]. Table 4 outlines the representative marginal distributions utilized to initialize the trade studies.

Table 4. Representative marginal distributions for Monte Carlo inputs.

Parameter	Distribution type	Mean (μ)	Standard deviation (σ)	Notes/units
$C_{NRE,AM}$	Normal	150,000 USD	25,000 USD	AM non-recurring engineering cost
$C_{U,AM}$	Lognormal	3,500 USD	600 USD	AM unit manufacturing cost
$C_{U,CM}$	Lognormal	4,200 USD	500 USD	Conventional unit manufacturing cost
λ_{AM}	Weibull (effective rate)	1.0×10^{-6} h^{-1}	0.2×10^{-6} h^{-1}	AM effective failure rate over mission
λ_{CM}	Weibull (effective rate)	0.8×10^{-6} h^{-1}	0.1×10^{-6} h^{-1}	CM effective failure rate over mission
$C_{L,AM}$	Normal	15,000 USD	3,000 USD	AM logistics/sustainment cost (program-specific)
$C_{L,CM}$	Normal	20,000 USD	4,000 USD	CM logistics/sustainment cost (program-specific)

Because advanced manufacturing processes exhibit programmatic dependencies, these variables cannot be assumed independent. Complex, high-performance electronics geometries drive concurrent increases in process optimization timelines, non-recurring engineering costs, and early defect risks. To replicate these physical realities, rank correlation structures were integrated via a Gaussian copula utilizing the Spearman correlation coefficients ($\boldsymbol{\sigma}$) detailed in Table 5, [14].

Table 5. Spearman rank correlation coefficients for Monte Carlo inputs.

Parameter Pair	σ	Physical Justification
C_NRE ↔ λ_AM	+0.65	Complex designs require more process development, increasing both NRE and defect risk
C_U ↔ λ_AM	+0.45	Higher-performance materials/processes cost more but may have immature reliability
C_NRE ↔ C_U	+0.30	Programs with high NRE often use specialized (costly) materials
λ_AM ↔ t_mission	−0.20	Longer missions drive more rigorous qualification, reducing field failure rates

5.2 Case Study 1: Conformal Low-Observable Antenna Array (LOAA)

The first validation case evaluates an X-band conformal phased-array antenna designed for a low-observable unmanned air vehicle (UAV), where planar PCBs housed inside heavy machined aluminum frames represent the conventional manufacturing baseline. In the AM workflow, a thin-walled ~0.5 mm conformal copper shell matching the aerodynamic profile of the UAV fuselage is fabricated via laser-based powder-bed fusion (LPBF). An aerosol-jet printing system subsequently deposits silver Ag nanoparticle ink directly onto the inner dielectric curves to create a monolithic feed network, eliminating discrete RF interconnects and fasteners, [4]–[6], [9].

To stabilize the underlying CBR metrics, strict design-for-additive-manufacturing (DfAM) guidelines were applied during the architecture phase. Overhang angles were mathematically constrained to minimize inaccessible internal support structures, suppressing post-process powder contamination and bounding the NRE cost C_NRE_AM. Critical internal RF propagation paths were explicitly oriented along the build axis to limit stair-stepping surface roughness, keeping skin-effect insertion losses within acceptable bounds, [4]. The resulting architecture achieved an 80–90% part-count reduction, a 20–25% reduction in overall mass, and a > 20dB reduction in radar cross-section (RCS) due to the seamless surface integration. Although the effective failure rate λ_AM was estimated to be ≈ 10 % higher than the conventional benchmark due to residual porosity and printed ink sintering variance, the aggregate benefit profile yielded a CBR index $\Psi > 1$, making the AM route highly preferred.

5.3 Case Study 2: Integrated Power-Distribution Module (IPDM)

The second case analyzes a high-power 500 W power-distribution module operating within a tactical ground vehicle environment. The conventional assembly relies on discrete, hand-formed copper busbars mechanically fastened across a standard machined aluminum heat sink block. The hybrid additive alternative synthesizes structural thermal-management optimization with printed electrical circuitry. An unconstrained topology-optimized AlSi10Mg lattice heat spreader featuring smooth, embedded internal microfluidic channels is built using LPBF, followed by multi-layer aerosol-jet deposition of Ag busbars insulated by intervening dielectric resin coatings [10], [12].

DfAM rules were paramount to mitigate interfacial delamination driven by coefficient of thermal expansion (CTE) mismatches under cyclic thermal loads. Thin, compliant polymer buffer films were introduced as graded stress-relief interfaces between the rugged LPBF metal base and the dense printed conductors [11]. Furthermore, uniform cross-sectional wall thicknesses were enforced across the geometric lattice cells to ensure uniform cooling gradients, preventing localized porosity concentrations and structural warping during post-build thermal processing [14]. This unified methodology dropped component counts by 80–85%, cut thermal resistance by 15–20% to stabilize hot-spot junctions, and reduced assembly labor hours by 60–70%. Even with a ~10% reliability penalty assigned to the printed dielectric interfaces, the considerable lifecycle savings and normalized unit cost reduction generated a decision index of $\Psi > 1$.

5.4 Case Study 3: Ruggedized Microwave Package (RMP)

The third case involves a high-frequency ruggedized microwave package subjected to intense ballistic shock profiles. The conventional baseline incorporates multiple micro-machined Kovar housings, separate microwave substrates, and separate mechanical interconnect assemblies. The advanced manufacturing alternative utilizes ceramic stereolithography (SLA) to print an integrated high-dielectric-constant alumina Al2O3 block housing embedded internal waveguide structures. The internal functional pathways are subsequently metalized via an electroless copper plating sequence.

The primary DfAM challenge for this ceramic workflow focused on liquid resin pooling and volumetric shrinkage during the UV-curing and subsequent sintering cycles. Blind internal channels were systematically converted into through-vias or augmented with specialized drain ports to ensure total evacuation of uncured slurry, avoiding internal geometry occlusions. Dedicated post-processing polishing allowances were integrated into the raw CAD model to allow chemical-mechanical polishing of critical internal waveguide walls, minimizing surface-roughness

attenuation [4]. This approach collapsed the overall housing part count by 70–80% while enhancing structural shock resilience. Despite a nominal +0 to +5% increase in initial unit manufacturing costs due to specialized post-cure firing schedules, the framework returned a value of $\Psi > 1$, establishing AM as a marginally preferred route specifically for low-volume, shock-critical deployments.

5.5 Case Study 4: On-Board Health-Monitoring Sensor (OHS)

The final case highlights an embedded structural health-monitoring node designed to capture in-flight strain and temperature parameters along a UAV wing assembly. While conventional sensing requires manual Routing, bonding, and hand-soldering of brittle fiber-optic lines and wire harnesses across the wing spar, the advanced method employs direct laser writing (DLW) to photopolymerize high-aspect-ratio microchannels directly into the primary component. Fiber-optic cables are mechanically dropped into these pre-formed channels and encapsulated with a tailored potting compound.

Standardized, co-printed material test coupons and witness structures were incorporated into the perimeter of the build envelope to monitor sub-micron process drift and verify local material compliance prior to wing installation [13]. This continuous process-verification protocol decreased sensor calibration drift, slashed manual assembly labor by 80–90% and eliminated redundant structural support brackets. Given the highly optimized and protected nature of the embedded fiber channels, the estimated MTBF was nearly equivalent to conventional routing ΔMTBF ~ -5% to 0%. Coupled with the massive reduction in wiring harness weight, the OHS configuration scored a high scalar benefit rating, leading to a decision index of $\Psi > 1$.

5.6 Cross-Case Analysis and Decision Uncertainty

A comprehensive cross-case baseline compiling the primary parameters across all four functional assemblies is structured in Table 6.

Table 6. Summary of case-study metrics for four electronic assemblies.

Metric	LOAA (Conformal Antenna)	IPDM (Power Module)	RMP (Microwave Package)	OHS (Health Sensor)
Primary AM/Hybrid Route	LPBF Cu + Inkjet Ag	LPBF Al + Inkjet Ag	Ceramic SLA + Plating	DLW Channels + Fiber
Part Count Reduction	~80–90%	~80–85%	~70–80%	~60–70%
Mass Reduction	~20–25%	~20–25%	~15–20%	~15–20%
Assembly Labor Cut	~30–40%	~60–70%	~30–40%	~80–90%
Unit Cost Change vs. CM	−5% to −10%	−10% to −15%	+0% to +5%	−10% to −15%
Estimated MTBF_AM vs MTBF_CM	≈ −10 % (slightly lower)	≈ −10 % (slightly lower)	≈ −10 % (slightly lower)	≈ −5 to 0 % (comparable)
CBR index Ψ (normalized)	>1 (AM preferred)	>1 (AM preferred)	≳1 (AM marginally preferred in shock-critical use)	>1 (AM strongly preferred, especially with SWaP emphasis)

To assess how input variability and correlation structures skew the viability of an advanced manufacturing selection, the total cost of ownership difference $\Delta TCO = TCO_{CM} - TCO_{AM}$ was calculated across the full Monte

Carlo spectrum for a manufacturing run of Q = 500 units. The resulting probability distribution is visualized in Figure 2. The statistical mean rests comfortably in positive territory, indicating that in approximately 76% of simulated program environments, the additive or hybrid workflow provides absolute financial and logistical cost savings over conventional machining and assembly options.

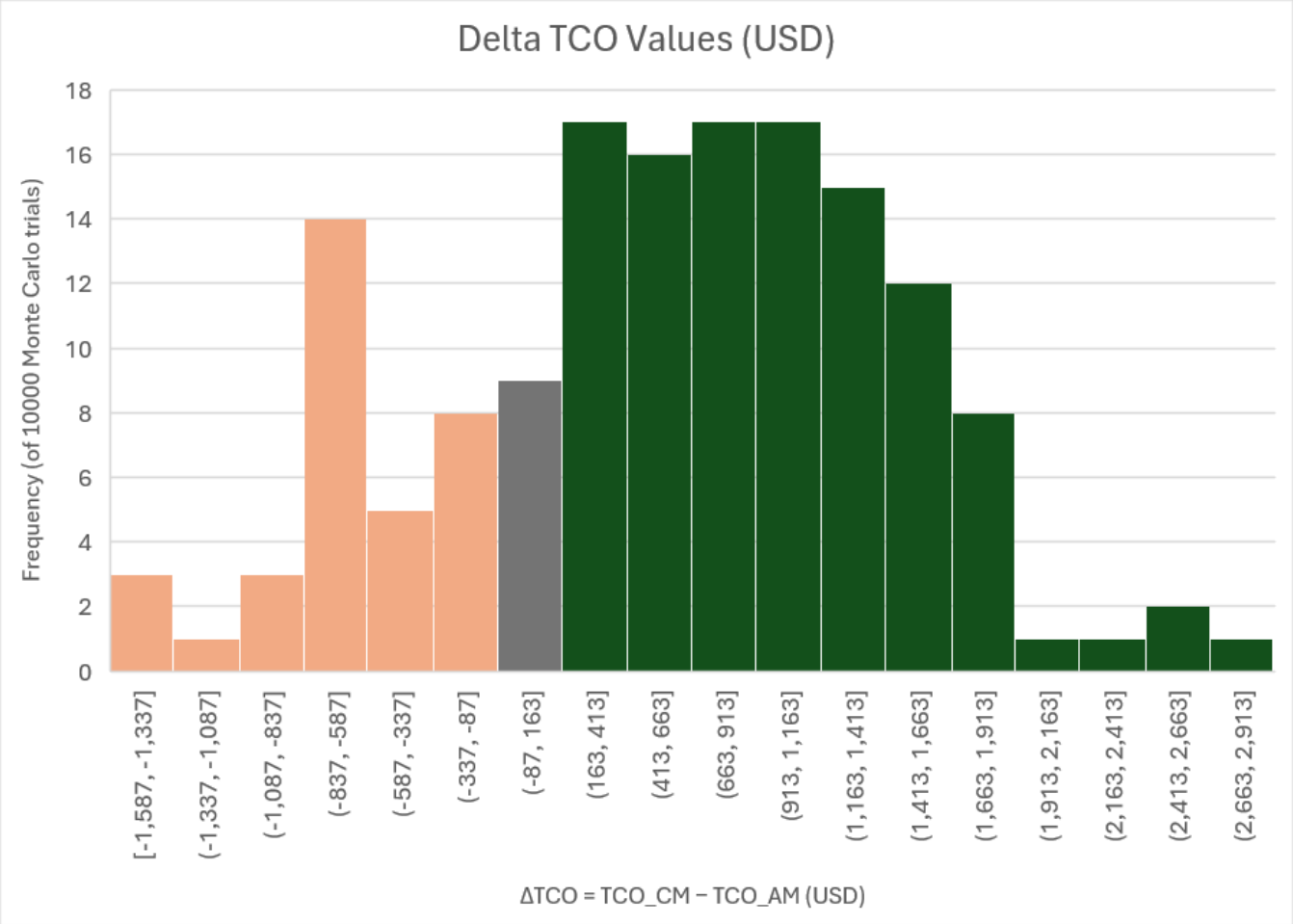


Fig. 2. Distribution of the total cost difference ΔTCO = TCO_CM − TCO_AM from a correlated Monte Carlo simulation (n = 10,000) for Q = 500 units. Positive values indicate scenarios where additive manufacturing offers lower total cost of ownership than conventional manufacturing; approximately 76% of samples fall in this region.

To isolate which operational or programmatic parameters exert the greatest leverage over decision confidence, variance-based global sensitivity analysis (Sobol indices) was executed directly against the simulation trials. The resulting sensitivity impacts are mapped via the tornado diagram in Figure 3.

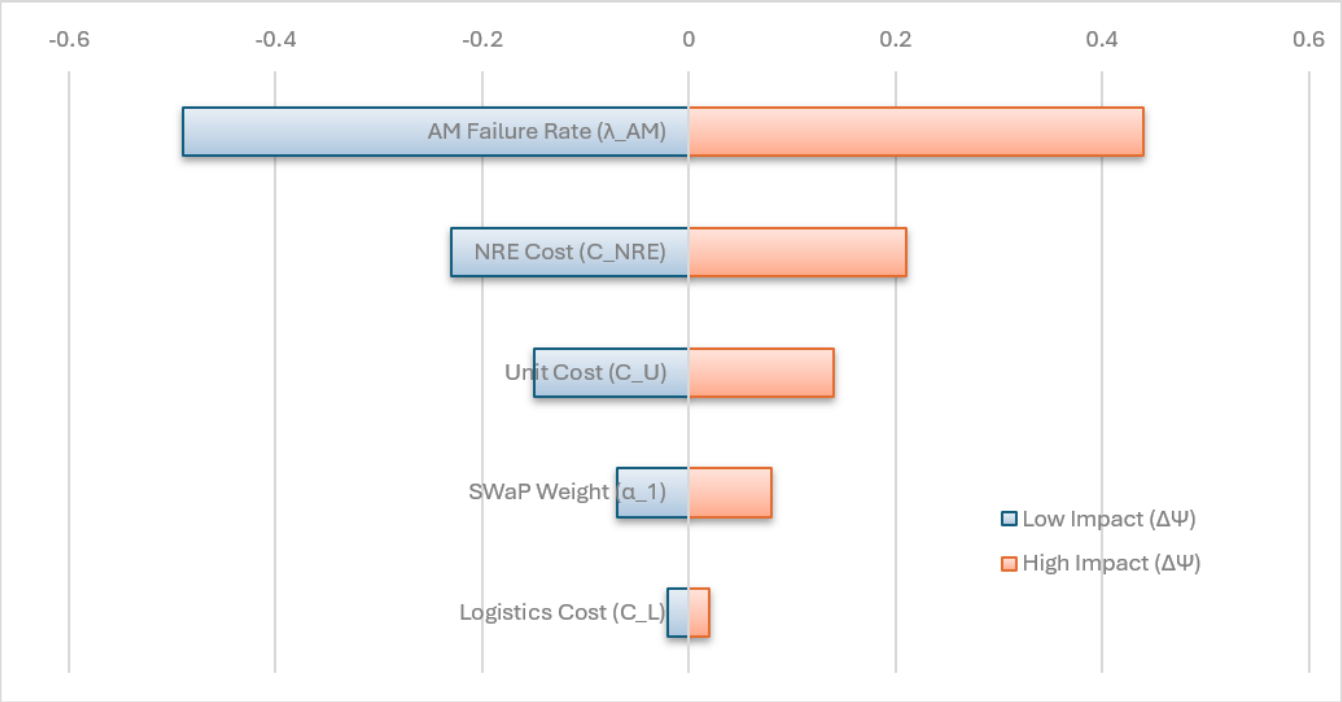


Fig. 3. Tornado diagram showing the impact of key input parameters on the CBR index Ψ. Bars indicate the change in Ψ when each parameter is varied over its uncertainty range. The model is most sensitive to AM failure rate λ_{AM} and AM NRE cost $C_{NRE,AM}$, identifying these as the primary levers for robust adoption of additive and hybrid manufacturing.

The structural model exhibits extreme sensitivity to changes in the effective AM failure rate λ_{AM} and the upfront non-recurring engineering costs $C_{NRE,AM}$, which combined account for approximately two-thirds of the total output variance in Ψ. Conversely, standard variations in conventional failure rates λ_{CM} and peripheral theater logistics costs C_L exert a negligible effect on the final index. Modeling these parameters as completely independent variables artificially deflates output variance and overestimates the true value of Ψ by approximately 10–15% for highly complex architectures. Consequently, isolating and driving down process variability via strict inline controls, standardized DfAM adherence, and targeted material qualification stand as the primary mechanisms to secure a robust business case for advanced electronics manufacturing.

6.0 RELIABILITY CONSIDERATIONS

AM and hybrid manufacturing routes introduce failure mechanisms that differ from those in traditional PCB and machined assemblies. Table 7 summarizes key AM-specific failure modes observed or reported in LPBF metals, printed conductors, and ceramic SLA parts, along with their root causes, impacts on electronic performance, and representative design-for-additive-manufacturing (DfAM) mitigations [3], [11], [13], [14]. These mechanisms and mitigations directly influence the effective AM failure rate $\boldsymbol{\lambda}_{AM}$used in the CBR framework.

Table 7. AM-specific failure modes and DfAM mitigations for electronic assemblies.

Failure mode	Root cause/process driver	Impact on electronic assembly	Representative DfAM / process mitigations
Porosity / incomplete fusion in LPBF metals	Insufficient laser energy density, improper scan speed or hatch spacing, poor	Reduced mechanical strength; increased RF loss; potential	Optimize LPBF process window (power, speed, hatch); use qualified powders; apply HIP; integrate coupons and in-situ monitoring to track porosity.

	powder quality [3], [14]	leak paths in fluid channels	
Anisotropic thermal expansion and residual stresses	Layerwise deposition, steep thermal gradients, constrained geometries [3], [14]	Distortion and warping; misalignment of interfaces; delamination at AM/printed interfaces	Design for uniform wall thickness; avoid abrupt section changes; add stress-relief features; use stress-relief heat treatments; include compliant interlayers at dissimilar material interfaces.
Surface roughness / stair-stepping	Layer thickness and contour strategy; partially fused particles on downskin surfaces [3], [4]	Increased RF insertion loss; field hot-spots; corrosion initiation sites	Orient critical RF and sealing surfaces to minimize stair-stepping; allocate post-processing stock; design for access to machining or polishing; use surface sealing/coating where appropriate.
Printed-conductor sintering defects (voids, microcracks)	Non-uniform ink deposition; solvent entrapment; suboptimal thermal or photonic sintering [2], [11], [15]	Increased resistance; drift under thermal cycling; early opens in feed networks or interconnects	Control ink rheology and deposition parameters; design pad and trace geometries for robust sintering; optimize sintering profiles; encapsulate critical traces; include in-situ test structures to monitor resistance drift.
Delamination at AM / printed interfaces	CTE mismatch between LPBF metal, printed conductors, polymers; poor surface preparation [3], [11]	Intermittent opens; degraded RF performance; moisture ingress along interfaces	Use graded or compliant interlayers (e.g., thin polymer films); design interconnect geometries to reduce peel stresses; control surface roughness and cleanliness before printing; apply appropriate primers or adhesion layers.
Contamination/ outgassing from AM materials	Residual binders or uncured resin in polymer/ceramic parts; trapped processing aids [13], [17]	Vacuum instability; dielectric drift; reliability degradation in sealed assemblies	Select materials with low outgassing; design geometries for solvent removal and bake-out; include vent paths where possible; perform thermal/vacuum conditioning; apply conformal coatings to isolate sensitive volumes.
Internal channel blockage or roughness	Powder entrapment in LPBF; inadequate depowdering; resin pooling in SLA channels [3], [17]	Reduced cooling efficiency; unpredictable flow; localized overheating	Design channels with appropriate diameters and access for depowdering; avoid blind channels; incorporate drain/vent features; validate channel integrity via CT or flow testing; adjust lattice and channel geometry for manufacturability.

Representative mechanisms include:

- **Porosity and incomplete fusion in LPBF metals,** arising from suboptimal laser power, scan speed, or powder feed, which can reduce mechanical strength and increase RF loss in waveguides and housings [3].
- **Anisotropic thermal expansion and residual stresses** due to layerwise deposition, which can lead to distortion, warping, and delamination at interfaces between AM metals and printed conductors or encapsulants [3], [14].
- **Surface roughness from stair-stepping or partially fused particles,** which can cause increased RF insertion loss, local field enhancement, and corrosion sites in RF and power structures [3], [4].
- **Sintering-related defects in ink-jet or aerosol-jet printed conductors,** including voids, incomplete coalescence, or microcracking, which can reduce conductor cross-section and lead to early failures under thermal cycling [2], [11].
- **Contamination and outgassing from residual binders or uncured resin** in polymer and ceramic AM parts, which can affect vacuum compatibility, dielectric stability, and long-term reliability [13], [17].

Mitigation strategies span process-parameter optimization, in-situ monitoring, post-processing (e.g., hot-isostatic pressing for LPBF metals, surface finishing, improved sintering schedules), and design measures such as compliant interlayers and controlled stress concentrators [3], [11], [13], [14]. These measures directly influence $\boldsymbol{\lambda}_{\mathrm{AM}}$in the CBR framework and hence the reliability factor $\boldsymbol{R}$.

Figure 4 summarizes the relationship between the AM and hybrid manufacturing process flow and the qualification activities required for high-reliability electronic assemblies. The horizontal blocks represent the main process stages: design and DfAM decisions (geometry, materials, interfaces); AM build operations (e.g., LPBF metals, ink-jet conductors, ceramic SLA); post-processing (heat treatment, sintering, machining, polishing, coating); coupon testing; inspection and in-situ monitoring; environmental testing (vibration, thermal cycling, humidity, shock); and finally, reliability modeling and the qualification decision.

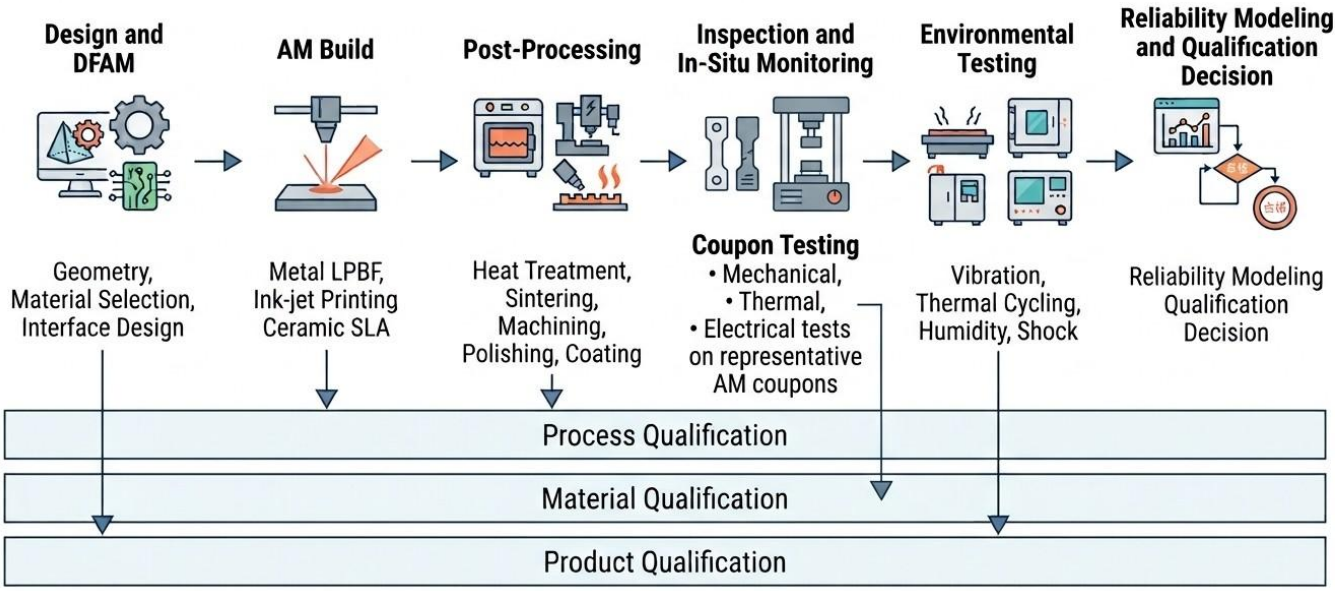


Fig. 4. Relationship between additive/hybrid manufacturing process stages and qualification activities for high-reliability electronic assemblies. The horizontal flow shows design and DfAM decisions, AM build, post-processing, coupon testing, inspection and in-situ monitoring, environmental testing, and reliability modeling.

Arrows link AM build and post-processing to process qualification, coupon testing to material qualification, and environmental testing to product qualification.

Beneath the process flow, the three qualification bands—process qualification, material qualification, and product qualification—indicate where each process stage contributes to establishing and maintaining reliability. Process-qualification activities (such as defining stable LPBF and ink-jet process windows and setting up process-control charts) are associated mainly with the AM build and post-processing stages [3], [13], [14]. Material qualification relies on coupon testing, where representative AM and hybrid materials and geometries are characterized for mechanical, thermal, electrical, and environmental properties under relevant stress profiles [7], [8], [11]. Product qualification and environmental stress screening (ESS) bring the full assembly through MIL-STD-style vibration, shock, and thermal-cycling profiles [7], [8], verifying that AM-specific failure modes identified in coupon and process studies are adequately controlled at system level. This flow highlights how upstream design decisions, process controls, and coupon-level evidence collectively influence the effective AM failure rate $\boldsymbol{\lambda}_{\mathrm{AM}}$ used in the CBR framework.

7.0 FUTURE DIRECTIONS

Several avenues can extend and generalize the framework presented here:

- **Multi-material and functionally graded AM:** Incorporating multiple materials (e.g., conductors, dielectrics, structural alloys) in a single build may enable richer integration but introduces new process-interaction and reliability challenges.
- **In-situ process monitoring and closed-loop control:** Integrating thermography, acoustic emission, or optical monitoring into AM processes can improve defect detection and support adaptive control strategies that reduce λ_AM and variability [14].
- **Machine-learning-assisted process and design optimization:** Using ML to map AM process parameters and design features to performance and reliability outcomes can augment the CBR framework and accelerate trade studies [15].
- **Expanded validation across platforms:** Applying the framework to broader sets of assemblies and platforms, including commercial high-reliability electronics, will help generalize weight choices, marginal distributions, and correlation structures.

8.0 CONCLUSIONS

This paper presented a reliability-aware Cost–Benefit–Reliability framework for evaluating additive and hybrid manufacturing routes against conventional manufacturing in high-reliability electronic assemblies. By combining an AM process and material taxonomy, a multi-criteria benefit metric, a TCO-based cost ratio, and a reliability factor derived from failure rates and qualification data, the CBR index enables quantitative comparisons under realistic program constraints.

Four case studies—conformal antenna housing, integrated power-distribution module, ruggedized microwave package, and embedded health-monitoring sensor—demonstrated that AM and hybrid routes can yield significant SWaP and integration benefits, reduced part count and assembly labor, and, in many cases, favorable or near-neutral TCO, provided that AM-specific reliability risks are mitigated through process optimization, DfAM, and qualification measures. A correlation-aware Monte Carlo analysis and global sensitivity study identified AM failure rate and AM NRE as dominant sources of decision uncertainty, suggesting that investments in reliability improvement and design/process reuse can materially improve the business case for AM adoption.

For low-volume, high-complexity, and highly integrated electronic assemblies, advanced manufacturing routes based on AM and hybrid processes can provide compelling value relative to conventional approaches. Embedding

reliability-aware design, process qualification, and data-driven decision tools such as the CBR framework into manufacturing workflows can accelerate the responsible deployment of AM in high-reliability electronics.

STATEMENTS & DECLARATIONS

The authors declare that no funds, grants, or other support were received during the preparation of this manuscript.

The authors have no relevant financial or non-financial interests to disclose.

All authors contributed to the study conception and design. Material preparation, data collection, and analysis were performed by Martin P. Goetz and Philip A. Lovell. The first draft of the manuscript was written by Martin P. Goetz and all authors commented on previous versions of the manuscript. All authors read and approved the final manuscript.

REFERENCES

[1] H. M. J. Al-Mosa, M. Ghassemi, and M. Razi, "A State-of-the-Art Review on 4D Printed Antennas and Other Adaptable Designs," IEEE Access, vol. 12, pp. 64293–64309, 2024. DOI: 10.1109/ACCESS.2024.3392811

[2] T. S. S. Prasad and R. K. Goyal, "The Evolution of Aerosol Jet Printing, A Review: Enhancing Micron-Scale Material Deposition," Advanced Materials Technologies, vol. 11, no. 2, Feb. 2026. DOI: 10.1002/admt.202501244

[3] W. E. Frazier, "Metal Additive Manufacturing: A Review," Journal of Materials Engineering and Performance, vol. 23, no. 6, pp. 1917–1928, Jun. 2014. DOI: 10.1007/s11665-014-0958-z

[4] Y. Cui, R. Bahr, S. A. Nauroze, T. Cheng, T. S. Almoneef, and M. M. Tentzeris, "3D Printed "Kirigami"-Inspired Deployable Bi-Focal Beam-Scanning Dielectric Reflectarray Antenna for mm-Wave Applications," IEEE Transactions on Antennas and Propagation, vol. 70, no. 9, pp. 7683-7690, Sept. 2022. DOI: 10.1109/TAP.2022.3177473

[5] A. G. Lopez et al., "Flexible and Scalable Additively Manufactured Tile-Based Phased Arrays for Satellite Communication and 5G mm-Wave Applications," in 2022 IEEE MTT-S International Microwave Symposium (IMS), Denver, CO, USA, 2022, pp. 495-498. DOI: 10.1109/IMS37028.2022.9865337

[6] O. A. C. Tas, "Additively manufactured high gain cavity backed Ku-band slot antenna," AEU - International Journal of Electronics and Communications, vol. 138, Art. no. 153746, Aug. 2021. DOI: 10.1016/j.aeue.2021.153746

[7] Department of Defense, Environmental Engineering Considerations and Laboratory Tests, MIL-STD-810H, Jan. 2019.

[8] Department of Defense, Test Method Standard: Microcircuits, MIL-STD-883L, Sep. 2019.

[9] K. N. Paracha et al., "Inkjet-Printed Antennas on Complex Conformal Surfaces Construction: Challenges and Future Prospects," IEEE Access, vol. 12, pp. 29339-29362, 2024. DOI: 10.1109/ACCESS.2024.3368297

[10] M. S. S. Danish, A. M. Blake, and J. W. Cook, "Economic and Supply Chain Viability of Additive Manufacturing for Low-Volume Spare Parts in Defense Logistics," Journal of Manufacturing Systems, vol. 68, pp. 112-125, June 2023. DOI: 10.1016/j.jmsy.2023.03.004

[11] H. Yu, X. Wang, and Y. Liu, "Reliability assessment and thermomechanical failure analysis of printed copper traces under accelerated thermal cycling," Reliability Engineering & System Safety, vol. 222, Art. no. 108412, June 2022. DOI: 10.1016/j.ress.2022.108412

[12] L. Wang, T. J. Eason, and S. Kumar, "Hybrid additive-subtractive manufacturing pathways for high-density power electronics packaging," Additive Manufacturing, vol. 55, Art. no. 102819, July 2022. DOI: 10.1016/j.addma.2022.102819

[13] S. Moylan, J. Slotwinski, and A. Cooke, "An Overview of Additive Manufacturing Standards Development," Proceedings of the ASME International Manufacturing Science and Engineering Conference, vol. 2, Art. no. V002T02A005, June 2014. DOI: 10.1115/MSEC2014-4112

[14] M. Khanzadeh, S. Chowdhury, M. Marufuzzaman, M. A. Tschopp, and L. Bian, "In-situ monitoring and defect detection in laser powder bed fusion using thermographic imaging," Journal of Laser Applications, vol. 30, no. 3, Art. no. 032002, Aug. 2018. DOI: 10.2351/1.5052736

[15] Y. Huang, L. Wang, and J. Zhang, "Machine Learning-Based Optimization of Process Parameters in Jet Printing of Conductive Inks," IEEE Access, vol. 10, pp. 48312-48325, 2022. DOI: 10.1109/ACCESS.2022.3171984

[16] J. Coykendall, M. Cotteleer, and J. Holdowsky, "3D opportunity in aerospace and defense: Additive manufacturing takes flight," Deloitte University Press, Tech. Rep., 2014.

[17] K. S. Babu, R. Rogers, and T. Harris, "Stereolithography of advanced structural ceramic components for space and aerospace hardware," Ceramics International, vol. 47, no. 14, pp. 19542-19553, July 2021. DOI: 10.1016/j.ceramint.2021.03.281